7-1-2015

Microdomain Formation, Oxidation, and Cation Ordering in $LaCa_2Fe_3O_{8+y}$

Patrick M. Price
Boise State University

Nigel D. Browning
Pacific Northwest National Laboratory

Darryl P. Butt
Boise State University

J. Am. Ceram. Soc., 98 [7] 2248–2254 (2015)
DOI: 10.1111/jace.13474

journal

Microdomain Formation, Oxidation, and Cation Ordering in $LaCa_2Fe_3O_{8+y}$

Patrick M. Price,[‡] Nigel D. Browning,[§] and Darryl P. Butt[‡,¶,†]

[‡]Department of Materials Science and Engineering, Boise State University, 1910 University Dr., Boise, Idaho 83725

[§]Fundamental and Computational Sciences Directorate, Pacific Northwest National Laboratory, 3335 Innovation Boulevard, Richland, Washington 99354

[¶]Center for Advanced Energy Studies, 995 University Boulevard, Idaho Falls, Idaho 83401

The compound $LaCa_2Fe_3O_{8+y}$, also known as the Grenier phase, is known to undergo an order–disorder transformation (ODT) at high temperatures and oxidation has been observed when the compound is cooled in air after the ODT. In this study, we have synthesized the Grenier compound in air using traditional solid-state reactions and investigated the structure and composition before and after the ODT. Thermal analysis showed that the material undergoes an ODT in both oxygen and argon atmospheres with dynamic, temperature dependent, oxidation upon cooling. Results from scanning transmission electron microscopy (STEM) suggest that the Grenier phase has preferential segregation of Ca and La on the two crystallographic A sites before the ODT, but a random distribution above the ODT temperature. Furthermore, STEM images suggest the possibility that oxygen excess may exist in La-rich regions within microdomains rather than at microdomain boundaries.

I. Introduction

There has been a great interest in lanthanum calcium ferrite LCF materials for potential applications as oxygen conducting membranes in high-temperature electrochemical devices due to their excellent chemical and thermal stability.[1–6] Despite this interest, the LCF material system is not fully understood. This is due, in part, to limitations in the ability to adequately characterize these materials using diffraction techniques. The structural similarity of the multiple phases present in the system result in the convolution of peaks in diffraction patterns and an order–disorder transformation (ODT) in Ca-rich specimens results in a quenched microstructure, which deceptively gives a cubic diffraction pattern.[7–14]

Three distinct crystal structures exist in the LCF system: ABO_3 (perovskite), $A'A_2B_3O_8$ (Grenier), and $A'_2B_2O_5$ (brownmillerite). The Grenier and brownmillerite phases may be considered derivatives of the perovskite structure with ordered oxygen vacancies in the pseudo-cubic [101] direction. The difference between the three structures (Fig. 1) is illustrated in the stacking sequence octahedra (O) and tetrahedra (T) given as follows: OOO (perovskite), OOT (Grenier), and OTOT' (brownmillerite). Almost identical planes of octahedra are common to all three crystal structures, allowing for the seamless stacking of multiple crystal structures, called intergrowths, by sharing of a common octahedral plane. Intergrowth structures in the LCF system were first observed in the early 1980s using high-resolution transmission electron microscopy.[7,11]

Lanthanum ferrite ($LaFeO_3$) has the perovskite structure. When Ca^{2+} is substituted for La^{3+} on the A site, a charge imbalance is introduced, which can be compensated by the formation of disordered oxygen vacancies or the increase in valance of iron from Fe^{3+} to Fe^{4+}. Both charge compensating methods have been shown to exist, allowing for variable nonstoichiometry of oxygen content in the material.[14] When the concentration of Ca exceeds the solubility limit in the perovskite structure, a second phase (Grenier) is formed as a result of the ordering of oxygen vacancies and formation of tetrahedral layers.

When quenched from 1400°C in air, the $LaCa_2Fe_3O_8$ compound gives cubic perovskite diffraction pattern and an increase in mass is observed, suggesting the transformation of tetrahedra to octahedra via the disordering of oxygen vacancies. However, high-resolution transmission electron microscopy revealed a more complicated microstructure, which suggested that microdomains of ordered oxygen vacancies persist in the material with sizes on the order of tens of nanometers.[15] A model was proposed in which the axis normal to ordered oxygen vacancies of each microdomain could be permuted in three mutually orthogonal directions producing a structure that is metrically cubic.[15] It was also suggested that the observed mass gain was due to the oxidation of domain walls upon cooling and that the structure observed in quenched phases was representative of the high-temperature structure.[15] In a separate investigation by Gibb,[16] $LaCa_2Fe_3O_8$ samples were quenched at different rates, resulting in different amounts of oxidation, with the least amount of oxidation with the fastest quench. Gibb also demonstrated that Mossbauer spectroscopy of quenched samples indicated the formation of microdomains; however, he suggested that this did not preclude the existence of a different structure at high temperatures.

In the work presented here, we have synthesized the $LaCa_2Fe_3O_8$ Grenier phase in air using solid-state ceramic processing techniques. We have revisited the ODT, oxidation, and microdomain structure using modern instruments. Simultaneous differential scanning calorimeter (DSC) and thermogravimetric analysis (TGA) was used for the *in situ* investigation of phase change energies and measurements of dynamic oxidation with submicrogram resolution. In addition, high-resolution microscopy has progressed significantly since the time of earlier investigations.[15,16] Scanning transmission electron microscopes (STEM) equipped with aberration correction and high-angle annular dark field (HAADF) detectors are capable of achieving subangstrom resolution, with z-contrast imaging and electron energy loss spectroscopy (EELS).[17–21]

II. Experimental Procedures

The $LaCa_2Fe_3O_8$ compound was synthesized using solid-state reactions. Stoichiometric portions of calcium carbonate

P. Davies—contributing editor

Manuscript No. 35497. Received August 19, 2014; approved December 22, 2014.
[†]Author to whom correspondence should be addressed. e-mail: darrylbutt@boisestate.edu

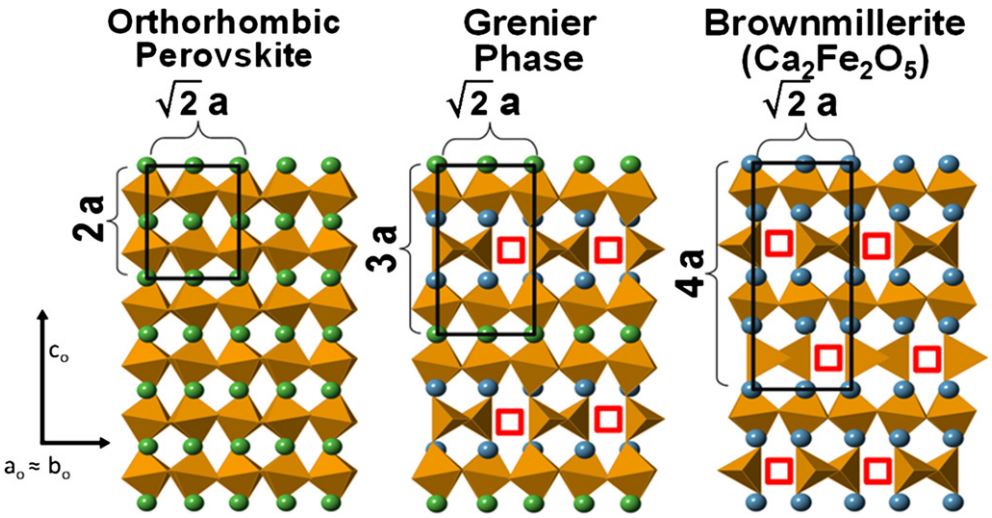

Fig. 1. Relationship between the orthorhombic perovskite, Grenier, and brownmillerite crystal structures. The red squares represent ordered oxygen vacancies.

(Puritronic® $CaCO_3$, 99.99% pure metals basis, Ward Hill, MA), iron (III) oxide (Fe_2O_3, 99.995% pure), and lanthanum (III) oxide (Reacton® La_2O_3, 99.999% pure, Ward Hill, MA) were combined to achieve the desired composition. Lanthanum oxide is hygroscopic and reacts with moisture in the air to form $La(OH)_3$.[22] The moisture content of each precursor powder was determined and corrected for by loss on ignition measurements by thermogravimetric analysis (Netzsch STA-449, Burlington, MA) prior to mixing each batch. Precursor powders were then mixed with yttria-stabilized zirconia media and isopropyl alcohol in nylon jars for 12 h on a table top mixer, and subsequently calcined at 1000°C for 8 h in a box furnace. The calcined powder formed a cake-like compact, which was crushed and then mixed as described above for an additional 10 h. The calcined mixture was dried and isostatically pressed into green pellets. The pellets were sintered in air at 1250°C for 24 h. The sintered pellets were then crushed, ground to a fine powder with a mortar and pestle, and then repressed and resintered for another 24 h. The pellets were recrushed, pressed, and sintered a total of 6 times to ensure homogeneity. The orthorhombic structure of synthesized samples was verified using X-ray diffractometer (Bruker AXS D8, Madison, WI) with parallel beam geometry. Diffracted intensities and peak positions were consistent with the indexed patterns of Hudspeth *et al.*[23]

All thermal analysis experiments were performed in a STA-449 (Netzsch STA-449) equipped with a simultaneous differential scanning calorimetry and thermogravimetric analysis (DSC-TG) carrier, silicon carbide furnace, alumina protective tube, and 85 μL platinum rhodium (Pt/Rh) crucibles. Temperature calibrations were performed via the melting of pure In, Sn, Bi, Zn, and Ag. Correction files with empty crucibles were obtained prior to all DSC-TGA experiments to remove background and noise from the sample signal. An empty crucible was used as a reference for all measurements.

Scanning transmission electron microscopy (STEM) was performed on a FEI Titan 80-300™ (FEI, Hillsboro, OR) equipped with a CEOS hexapole spherical aberration corrector (Corrected Electron Optical Systems GmbH, Heidelberg, Germany) for the probe forming lens, HAADF detector, and a high-resolution Gatan Imaging Filter for EELS (Gatan, Pleasanton, CA). Samples for STEM were prepared on a FEI Quanta dual FIB/SEM.

III. Results and Discussion

The change in mass as a result of the oxidation after ODT was measured in quenched specimens in previous investigations.[15,16] In the work presented here, we have measured the change in mass with thermogravimetric analysis and found that the oxidation behavior during cooling is dynamically dependent on temperature and reversible upon heating. The thermogravimetric analysis data in Fig. 2 shows the change in mass of the $LaCa_2Fe_3O_8$ Grenier compound before and after the order–disorder transition. There is a small mass loss (0.3%) when the sample is heated to 1360°C due to the increase in thermally created oxygen vacancies. When the sample undergoes the endothermic ODT, there is a characteristic 0.06% increase in mass that always occurs when heated in air. As the sample is cooled to 500°C there is a comparatively large increase in mass due to oxygen uptake in the material. The oxygen content is stabilized by the formation of octahedra from tetrahedra and stoichiometric conversion of $Fe^{3+} \leftrightarrow Fe^{4+}$, as found in oxygen-deficient perovskites. When the ramp is halted in the isothermal region at 500°C, oxidation stops. Likewise, when the specimen is heated to 600°C, the oxygen gained during cooling is released as indicated by a proportional mass loss. This same behavior is observed when the temperature is reduced back to 500°C and then backup to 700°C. The temperature-dependent oxygen uptake and release behavior suggests that the situation is

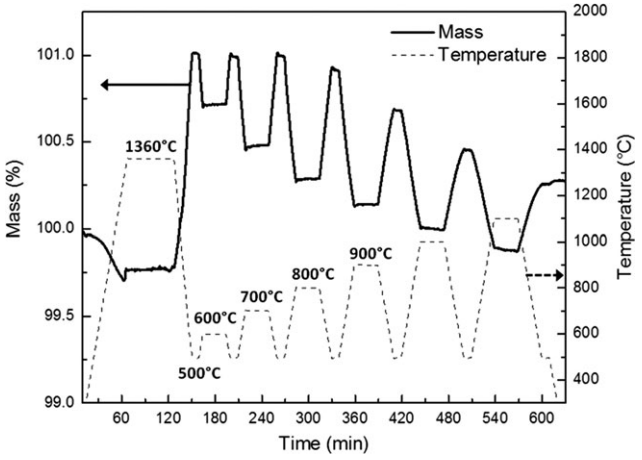

Fig. 2. Thermogravimetric analysis (solid line) of the oxidation behavior before and after the order–disorder transformation. After quenching the temperature (dashed line) is cycled from 500°C to increasingly higher temperatures to illustrate the dynamic oxidation behavior and the stability of the microdomains at lower temperatures.

more complicated than a simple oxidation of domain walls. An alternative explanation is the formation of a material with a larger equilibrium concentration of thermally activated oxygen vacancies when the $LaCa_2Fe_3O_{8+y}$ compound is quenched. When the temperature is cycled from temperatures 800°C or higher, there is a systematic decrease in the amount of oxidation of the material when the temperature is returned to 500°C, indicating a restructuring of the material back to the starting $LaCa_2Fe_3O_8$ compound.

Previous investigations have focused on the oxidation after the ODT in samples treated in air. The thermogravimetric data in Fig. 2 indicates there is little to no gain in mass at the ODT temperature and that oxidation does not begin until the sample is cooled. As no oxygen is required during the ODT, it suggests that Grenier compounds treated in oxygen-deficient atmospheres may also undergo the ODT. The ODT and oxidation behavior of the $LaCa_2Fe_3O_{8+y}$ compound treated in an oxygen-deficient atmosphere are shown in the TG/DSC data in Fig. 3. The Grenier specimen was heated to 1360°C and then cooled to 500°C in high-purity argon. An endothermic peak at in the DSC signal at approximately 1300°C confirms that the ODT also occurs in oxygen-deficient atmospheres. An exothermic peak is present in the DSC signal during cooling, indicative of a structural reconfiguration. At 500°C, oxygen is introduced for the first time in the form of clean air, resulting in the immediate oxidation of the Grenier compound to a mass above that of the starting material. The temperature is then increased to 700°C and then decreased to 200°C, resulting in the same temperature-dependent oxygen uptake and oxygen release observed in Grenier specimens treated in air. This suggests that Grenier specimens treated in oxygen-deficient atmospheres result in a similar microdomain structure as those treated in air and that oxidation is a result of the microdomain structure, rather than the formation of the microdomain structure as a result of oxidation.

The temperature-dependent oxidation of the Grenier compound is evident in the TG/DSC data presented in this study and previous studies have shown the existence of ordered oxygen vacancies and microdomain texture[15]; however, it remains unclear if this is representative of the Grenier compound above the ODT temperature. To gain insight into this question, the starting $LaCa_2Fe_3O_8$ Grenier compound was heated above the ODT temperature in air, quenched, and reheated above the ODT temperature in two subsequent cycles as shown in the TG/DSC data in Fig. 4. In the first cycle, the characteristic endothermic peak is present in the DSC signal with the small characteristic increase in mass shown in the TG signal during the ODT. On cooling, there is also an exothermic peak in the DSC signal indicative of

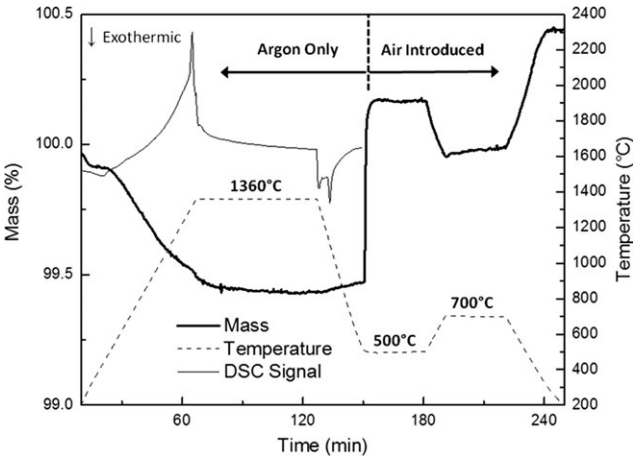

Fig. 3. Thermogravimetric analysis of the oxidation behavior after treatment in argon. Clean air is introduced after quenching at 500°C resulting in oxidation of the sample.

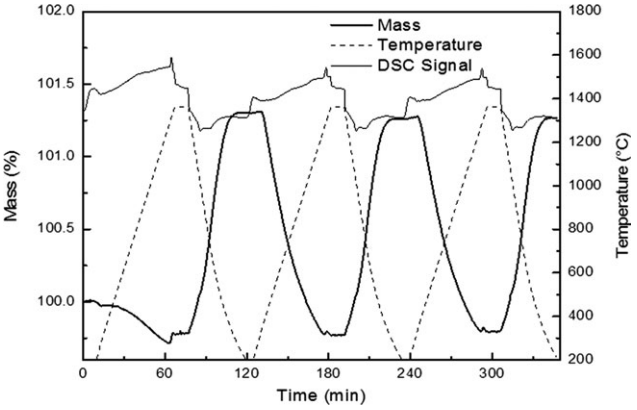

Fig. 4. Thermogravimetric analysis of the oxidation behavior after repeated heat treatments above the order–disorder transition temperature.

restructuring. On both of the subsequent heating and cooling cycles, both the endothermic and exothermic peaks are present in the DSC signal and the oxidation behavior is almost identical to the initial heating and cooling cycle. This suggests the high-temperature structure is not retained and that the microdomain structure must reorder during the ODT.

The DSC signals from both Figs. 3 (argon) and 4 (air) are plotted as a function of temperature in Fig. 5 and tabulated in Table I. The order–disorder transition temperature was found to be slightly higher in argon atmospheres than in air. The ODT temperature measured from the second and third cycles in air were slightly lower than the first. The lowering of the phase transition temperature may be due to the lowering of the energy barrier due to the presence of available oxygen. The DSC signals in the upper region of Fig. 5 show an exothermic peak observed during cooling, indicative of a reconstructive transformation. There is a large difference in the exothermic peak shape and position between samples treated in air and argon. The exothermic peak of the argon-treated sample has a sharper peak and occurs at a temperature ≈100°C higher than air-treated samples, indicating the presence of excess oxygen may act to impede the phase transition during cooling.

It is evident in the DSC and thermogravimetric data that:

1. The room-temperature microdomain structure is not likely representative of the high-temperature

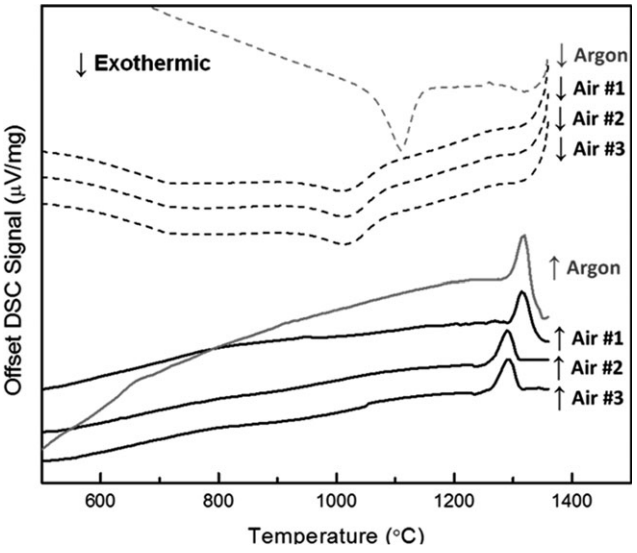

Fig. 5. Comparison of endothermic DSC signals during the order–disorder transformation and the exothermic peaks suggesting a structural rearrangement during cooling.

Table I. Order-Disorder Transformation Temperatures Measured by DSC

Run	Type	DSC Onset (°C)±15°C	DSC Peak (°C)±5°C
Argon	Heating	1288	1318
Air cycle #1		1285	1312
Air cycle #2		1236	1291
Air cycle #3		1236	1292
Argon	Cooling	1163	1109
Air cycle #1		1083	1009
Air cycle #2		1083	1013
Air cycle #3		1083	1013

(< 1320°C) structure based on the exothermic peaks observed in the DSC data upon cooling and the endothermic peaks of the quenched microdomain structure on subsequent reheating.
2. The quenched microdomain structure is oxidized on cooling resulting in an increase in the oxygen stoichiometry above that of the starting material.
3. The microdomain structure is likely present in Grenier compounds treated in both oxidizing and oxygen deficient atmospheres above the ODT temperature, based on the oxidation behavior shown in Figs. 2–4.
4. The oxidized microdomain sample can be returned to the starting oxygen stoichiometry by annealing the material above 700°C.

To help elucidate the cause of the dynamic temperature-dependent oxidation behavior, aberration corrected STEM was used to investigate the structure of the $LaCa_2Fe_3O_{8+y}$ Grenier phase treated above and below the ODT temperature. The STEM image of the low-temperature Grenier compound with a pseudo cubic [100] zone axis is shown in Fig. 6(a). While the oxygen atoms cannot be visualized directly in this image, the iron atoms located in the tetrahedra planes are physically offset as shown in the superimposed crystal structure, allowing for the distinction between planes octahedrally and tetrahedral coordinated iron. There are two unique crystallographic A sites in the orthorhombic $P2_1ma$ space group.[23] Broadening of peaks in Mossbauer studies of the Grenier compound led Gibb to conclude that different coordination states of iron atoms were present and that the Ca and La A-site cations were randomly distributed throughout the structure.[16]

A STEM image of the starting Grenier compound is shown in the left side of Fig. 6. The two crystallographic A sites are indicated by the green and blue spheres in the superimposed crystal structure in the top-left corner. The green A site sits between two planes of octahedra and the blue A site sit between a plane of octahedra and a plane of tetrahedra. The STEM image of the left has a bright row of atomic columns on the green site and darker atomic columns on all of the blue sites. The *z*-contrast afforded by the HAADF detector suggests that the green A site located between octahedral planes is preferentially substituted by the larger lanthanum ($Z = 57$) over the calcium cation ($Z = 20$). The z-contrast can be extended to show that the intensity of the iron cations ($Z = 26$) are, on average, brighter than the adjacent A sites believed to be preferentially occupied by calcium. If the larger lanthanum cation was randomly on the blue A site, the average intensity would be predicted to be periodically higher than adjacent iron columns. The preferential occupation of lanthanum between octahedral planes is also confirmed in the EELS superimposed over the Grenier phase shown in Fig. 7.

A STEM image of the quenched microdomain structure is shown on the right-hand side of Fig. 6, which is also oriented with a pseudo cubic [100] zone axis. For ease of comparison, the tetrahedral planes of the two STEM images in Fig. 6 are lined up. It is evident from the random distribution of *z*-contrast across the two A sites in the STEM image, that lanthanum and calcium are randomly distributed on the two crystallographic sites in the quenched microdomain structure.

The STEM image shown if Fig. 8 is that of a single microdomain oriented with a pseudo cubic [100] zone axis. The white tick marks on the top and bottom identify the planes of tetrahedra in the structure. There are no stacking faults or disruption of the periodicity of the spacing of the tetrahedral planes horizontally; however, the characteristic offset of the iron cations in the tetrahedral plane disappear in a domain on the right side of the image. The FFT for this region is shown on the right, indicating cubic symmetry. In contrast, the FFT from the left side of the image contains additional superlattice reflections indicating the characteristic tetragonal symmetry of the cations in the Grenier compound. The images on the lower left and right side of Fig. 8 are of the original *z*-contrast STEM image with a threshold subtraction adjusted so pixels equal to or less than the intensity of iron cations are removed from the image. The remaining atomic

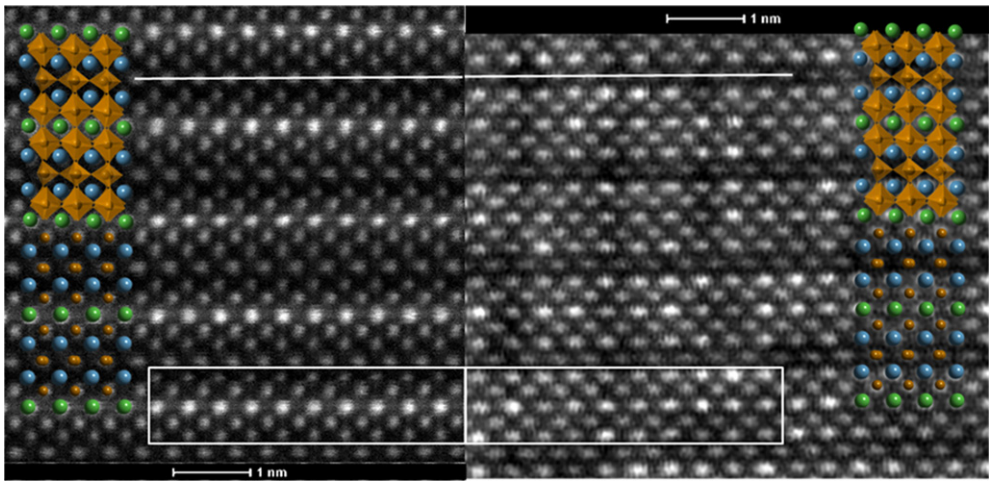

Fig. 6. STEM images used for the comparison of the structure before (left) and after (right) the order–disorder transformation. The two micrographs are situated so that tetrahedral planes are lined up as indicated by the horizontal white lines at the top of the image. The *z*-contrast seen in the Grenier compound on the left indicates A-site cation ordering where the bright A-site positions (green spheres) are preferentially substituted by La and the darker A-site positions (blue spheres) are preferentially occupied by Ca. The *z*-contrast seen in the image on the right (microdomain structure) indicates the random occupation of La and Ca on the A sites based on the random contrast of A-site positions. The smaller brown spheres indicate the position of the iron atoms.

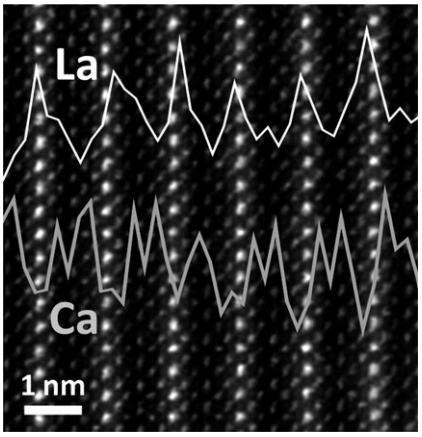

Fig. 7. STEM image of Grenier phase with overlaid EELS core-loss signal. The EELS data show that the bright columns are preferentially occupied by lanthanum whereas the A-site locations on either side of the tetrahedra are preferentially occupied by calcium.

areas of bright contrast are representative of atomic columns that have an average *z*-contrast greater than iron and therefore contain higher concentrations of lanthanum. The quantity of remaining bright pixels in the image was quantified with digital micrograph. There are approximately 20% more bright pixels on the right side of the image. While this analysis is semiqualitative, it suggests that the region with cubic symmetry in the otherwise uninterrupted periodicity of tetrahedral planes of a single microdomain has a higher lanthanum concentration than the area on the left. This suggests that oxidation may occur at lanthanum-rich regions throughout the material. This is supported by the fact that no ordered oxygen vacancies have been observed in lanthanum ferrite compounds. It has been demonstrated that lanthanum ferrite will maintain the perovskite structure in extremely reducing atmospheres, and will decompose prior to the formation of ordered oxygen vacancies.[24]

It was originally proposed by previous authors that the oxygen excess observed in quenched microdomain samples was located in the domain wall.[12] Other authors have analyzed microdomain boundaries in other systems with STEM and EELS and found no evidence of oxidation at domain boundaries.[22] The STEM image in Figs. 6–8 clearly demonstrate the transition from a preferentially occupied state of A-site cations, with lanthanum stabilized between two octahedral planes, to a random distribution of the two A-site cations in the microdomains structure. It is unlikely that clusters of lanthanum will be able to stabilize the ordered oxygen vacancies at room temperature and offer an alternative explanation as to where oxidation occurs in the microdomains texture of quenched Grenier compounds.

The oxidation as a result of lanthanum clustering is supported by two other observations. First, the thermogravimetric data in Fig. 2 show that the oxidation behavior is stable until the sample is annealed at temperatures greater than 700°C. Oxygen is mobile well below 700°C, suggesting that the reconstruction of the low-temperature Grenier compound is likely limited by cation diffusion. Second, if the La^{3+} cations are randomly distributed, then 1/3 would be expected to reside between octahedral planes and 2/3 would be expected to reside in between octahedral and tetrahedral planes. Therefore, clusters of La^{3+} cations residing on the Ca^{2+} sites would need to be locally stabilized by excess oxygen. One oxygen anion (O^{2-}) will compensate for the local charge difference created by every two La^{3+} cations. This would result in a minimum expected oxidation stoichiometry increase of $y = 0.33$ giving $LaCa_2Fe_3O_{8.33}$. The measured mass gain from thermogravimetric data in samples quenched in air was 1.29%, suggesting an estimated stoichiometry increase to $LaCa_2Fe_3O_{8.41}$, which is in good agreement with the expected value. The redistribution of lanthanum clusters to an ordered state gives a phenomenological explanation as to the reason for the oxidation in the microdomain structure. It is important to note that this domain structure is a result of the reconstruction of the high-temperature phase upon cooling.

The STEM imaging technique was also used to investigate microdomain boundaries. The high-resolution STEM image in Fig. 9 shows a typical microdomain texture reminiscent of those reported by previous authors.[15] The authors suggested that the microdomain texture was the result of the permutation of the OOT stacking sequence of the Grenier phase in three mutually orthogonal directions. The atomic resolution micrograph shown in Fig. 9(b) shows an additional level of complexity. The tetrahedral planes in the two microdomains at the top and bottom of the image are oriented in the same

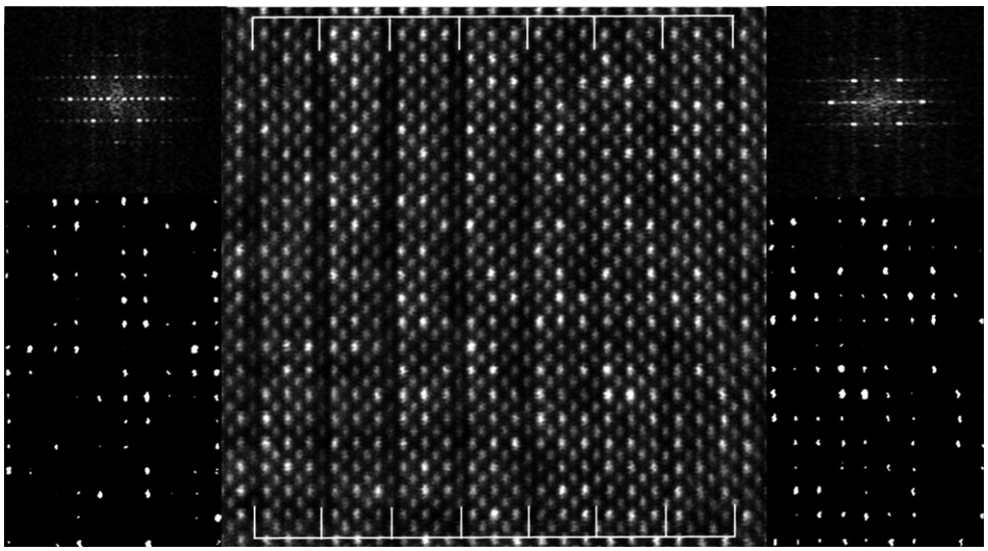

Fig. 8. A STEM image of a single microdomain with a [100] view direction. The region on the right side has a cubic symmetry as indicated by the FFT on the right. The FFT from the left side of the image gives the expected tetragonal symmetry of the cations in the Grenier structure. The white tick marks at the top and bottom illustrate the periodicity of the tetrahedral planes. The results of a threshold subtraction are shown on the sides. Image analysis reveals a 20% increase in the number of bright pixels on right side of the STEM image, indicating a higher concentration of lanthanum.

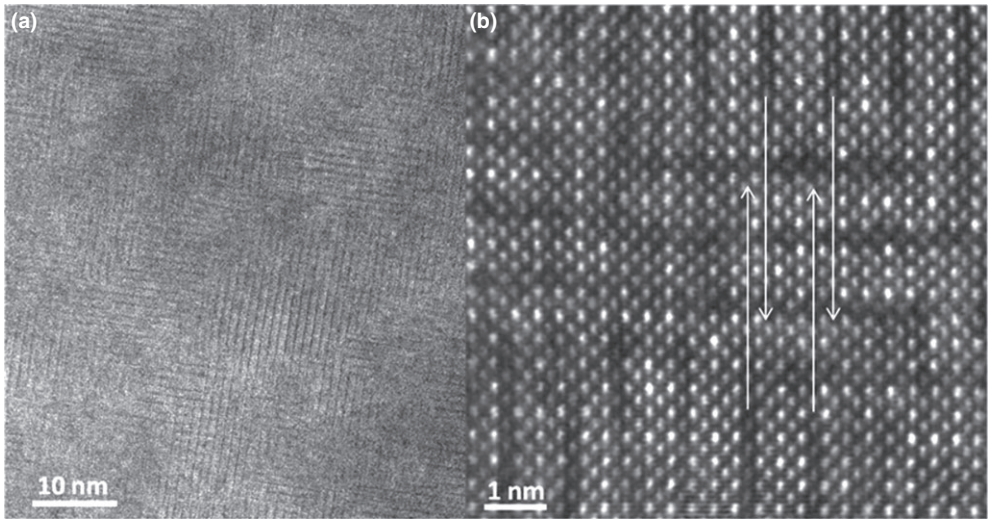

Fig. 9. STEM image of the [100] zone axis of (a) typical microdomain structure and (b) a stacking mismatch of tetrahedral planes in the microdomain texture Ordered oxygen vacancies form orthogonally to compensate for the mismatched stacking of the vertical ordered vacancies.

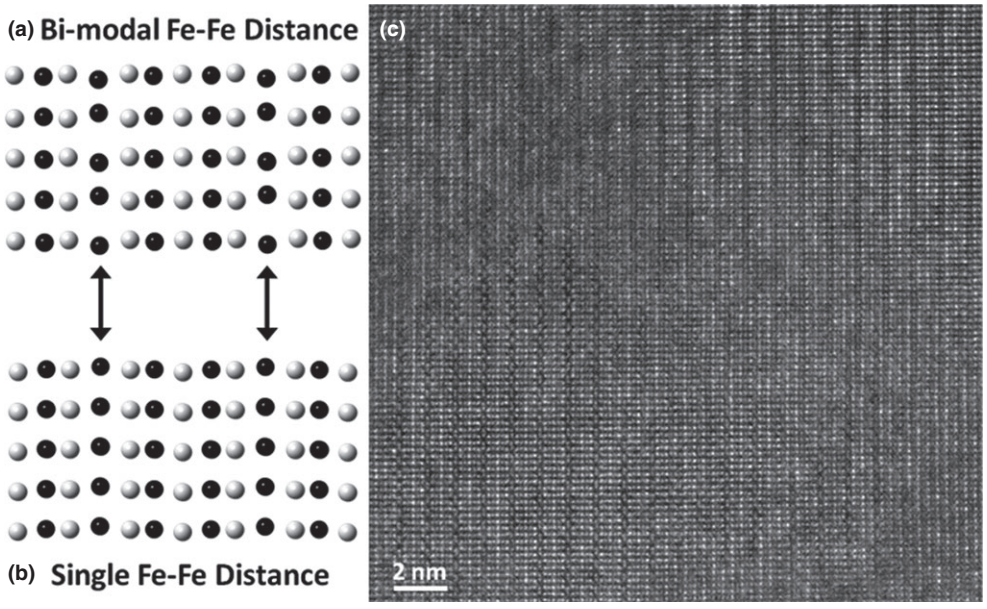

Fig. 10. Crystallographic representation of the crystal structure (a) viewing down the pseudo cubic [101]. The Fe–Fe distance alternates between long and short as shown in the planes indicated by the arrows. (b) viewing down the [$\bar{1}$01] zone axis. The Fe–Fe distance is fixed (c) STEM image showing microdomains in the [101] type orientation with both crystallographic variations present. The bimodal iron separation can be seen on the lower left and the equally spaced iron cations are located in the upper-right corner.

direction, but are offset by a single plane as indicated by the arrows. Rather than the tetrahedral planes converging to form a stacking of two consecutive tetrahedra, a small microdomain forms orthogonally between the two. This was representative of most of the area of the microdomains when viewed from the [100] type direction. Most of the tetrahedral planes were oriented in one direction with only small domains oriented orthogonally separating mismatched tetrahedral planes.

A view of microdomain formation with a pseudo cubic [101] zone axis is shown in Fig. 10. Unlike the [100] zone axis, which is equivalent when rotated 90°, the [101] zone axis changes Fe–Fe bond lengths when rotated. Ordered oxygen vacancies are located parallel to the [101] direction and the iron spacing alternates between long and short bond lengths. When rotated 90° to the [$\bar{1}$01] direction, the Fe–Fe distance is equal. Both of these variations are seen in the STEM image with the (a) variant located in the bottom-left corner and the (b) variant located in the top-right corner. A mismatch of tetrahedral planes is also commonly found in this image and throughout the structure. However, there was no orthogonal formation of oxygen vacancies visible in this direction. The simultaneous presence of the two variants suggests when the high-temperature phase undergoes the exothermic reconstructive transition during cooling, there is equal likelihood of formation of different crystallographic orientations next to each other. The random occurrence of similar crystallographic orientations further illustrates that the microdomain structure is not representative of the high-temperature phase and suggests that the microdomain texture may result, at least partially, from the mismatch of tetrahedral planes during the reconstructive transformation.

IV. Conclusions

Thermogravimetric analysis and DSC has revealed that the $LaCa_2Fe_3O_{8+y}$ Grenier compound undergoes a reconstructive phase transformation that is not retained in quenched

samples. During the quenching process, a dynamic temperature-dependent oxidation was observed, even in samples initially treated in oxygen-deficient atmospheres. High-resolution STEM images revealed the preferential occupation of lanthanum between octahedral planes and calcium between the octahedral and tetrahedral planes of the synthesized Grenier phase. In contrast, after quenching from above the ODT temperature the A-site cations were observed to be disordered in the microdomain structure. We propose that the disordering of the lanthanum cations may be the cause for the oxidation behavior. Evidence has been presented to support the possibility of oxidation of lanthanum clusters within microdomains rather than oxidation segregated to domain walls. We observed misalignment in the stacking of tetrahedral planes that may also give rise to the microdomain texture seen at lower magnifications. The oxidized microdomain structure appears to release and uptake oxygen very rapidly at temperatures as low as 400°C and is metastable at temperatures below 700°C, indicating that this material may be useful as a low temperature oxygen conductor. The structure of the high-temperature phase is still unknown.

Acknowledgments

A portion is part of the Chemical Imaging Initiative conducted under the Laboratory Directed Research and Development Program at Pacific Northwest National Laboratory (PNNL) and was performed in the William R. Wiley Environmental Molecular Sciences Laboratory (EMSL), a national scientific user facility sponsored by DOE's Office of Biological and Environmental Research and located at PNNL. PNNL, a multiprogram national laboratory, is operated by Battelle for the Department of Energy under Contract DE-AC05-76RLO1830. We would also like to thank Hao Yang, Michael Carolan, and Raymond Cutler for their help with this research.

References

[1]U. Balachandran, J. T. Dusek, R. L. Mieville, R. B. Poeppel, M. S. Kleefisch, S. Pei, T. P. Kobylinski, C. A. Udovich, and A. C. Bose, "Dense Ceramic Membranes for Partial Oxidation of Methane to Syngas," *Appl. Catal. A*, **133** [1] 19–29 (1995).

[2]J. A. Kilner, "Optimisation of Oxygen Ion Transport in Materials for Ceramic Membrane Devices," *Faraday Discuss.*, **134**, 9–15 (2007).

[3]P. S. Maiya, U. Balachandran, J. T. Dusek, R. L. Mieville, M. S. Kleefisch, and C. A. Udovich, "Oxygen Transport by Oxygen Potential Gradient in Dense Ceramic Oxide Membranes," *Solid State Ionics*, **99** [1–2] 1–7 (1997).

[4]V. V. Kharton, A. A. Yaremchenko, A. V. Kovalevsky, A. P. Viskup, E. N. Naumovich, and P. F. Kerko, "Perovskite-Type Oxides for High-Temperature Oxygen Separation Membranes," *J. Membr. Sci.*, **163** [2] 307–17 (1999).

[5]P. V. Hendriksen, P. H. Larsen, M. Mogensen, F. W. Poulsen, and K. Wiik, "Prospects and Problems of Dense Oxygen Permeable Membranes," *Catal. Today*, **56** [13] 283–95 (2000).

[6]P. N. Dyer, M. F. Carolan, D. Butt, R. H. E. V. Dooorn, R. A. Cutler and Air Products and Chemicals Inc, "Mixed Conducting Membranes for Syngas Production," U.S. Pat. 6,492,290, August 2002.

[7]M. Vallet-Regi, J. Gonzalez-Calbet, M. A. Alario-Franco, J. C. Grenier, and P. Hagenmuller, "Structural Intergrowth in the $Ca_xLa_{1-x}FeO_{3-x/2}$ System ($0 < x < 1$). An Electron-Microscopy Study," *J. Solid State Chem.*, **55** [3] 251–61 (1984).

[8]J. C. Grenier, M. A. Alario-Franco, J. M. Gonzalez-Calbet, and M. Vallet-Regi, "Brownmillerite-Type Microdomains in the Calcium Lanthanum Ferrites : $Ca_xLa_{1-x}FeO_{3-y}$ I. $2/3 < x < 1$," *J. Solid State Chem.*, **49**, 219–31 (1983).

[9]J. M. Gonzalez-Calbet, M. A. Alario-Franco, and M. Vallet-Regi, "Microdomain Formation – A Sophisticated Way of Accommodating Compositional Variations in Nonstoichiometric Perovskites," *Cryst. Lattice Defects Amorphous Mater.*, **16**, 379–85 (1987).

[10]J. C. Grenier, M. Pouchard, P. Hagenmuller, M. J. R. Henche, M. Vallet, J. M. C. Calbet, and M. A. Alario-Franco, "Order-Disorder Transition at High Temperature and Microdomain Formation in Oxidized Ferrites," *Mater. Res. Soc. Symp. Proc.*, **21**, 387–91 (1984).

[11]J. M. Gonzalez-Calbet, M. Vallet-Regi, M. A. Alario-Franco, and J. C. Grenier, "Structural Intergrowths in the Calcium Lanthanum Ferrites - $Ca_xLa_{1-x}FeO_{3-y}$ ($2/3 \leq x \leq 1$)," *Mater. Res. Bull.*, **18**, 285–92 (1983).

[12]M. A. Alario-Franco, M. J. R. Henche, M. Vallet, J. M. Gonzalez -Calbet, J. C. Grenier, A. Wattiaux, and P. Hagenmuller, "Microdomain Texture and Oxygen Excess in the Calcium-Lanthanum Ferrite : $Ca_2LaFe_3O_8$," *J. Solid State Chem.*, **46**, 23–40 (1983).

[13]J. M. Gonzalez-Calbet, M. Vallet-Regi, and M. A. Alario-Franco, "Microdomains in the Reduction of $Ca_2LaFe_3O_{8+y}$," *J. Solid State Chem.*, **60**, 320–31 (1985).

[14]P. M. Price, E. Rabenberg, D. Thomsen, S. T. Misture, and D. P. Butt, "Phase Transformations in Calcium-Substituted Lanthanum Ferrite," *J. Am. Ceram. Soc.*, **97**, 2241–5 (2014).

[15]M. A. Alario-Franco, M. J. R. Henche, M. Vallet-Regi, J. M. Gonzalez-Calbet, J. C. Grenier, A. Wattiaux, and P. Hagenmuller, "Microdomain Texture and Oxygen Excess in the Calcium-Lanthanum Ferrite : $Ca_2LaFe_3O_8$," *J. Solid State Chem.*, **46**, 23–40 (1983).

[16]T. C. Gibb, "An Investigation of Microdomains in $Ca_2LaFe_3O_8$ by Mossbauer Spectroscopy," *J. Solid State Chem.*, **74**, 176–83 (1988).

[17]S. J. Pennycook, "Z-Contrast Transmission Electron Microscopy: Direct Atomic Imaging of Materials," *Annu. Rev. Mater. Sci.*, **22**, 171–95 (1992).

[18]M. Varela, A. R. Lupini, K. Van Benthem, A. Y. Borisevich, M. F. Chisholm, N. Shibata, E. Abe, and S. J. Pennycook, "Materials Characterization in the Aberration-Corrected Scanning Transmission Electron Microscope," *Annu. Rev. Mater. Res.*, **35** [1] 539–69 (2005).

[19]M. Varela and S. J. Pennycook, "Ultramicroscopy Column-by-Column Compositional Mapping by Z-Contrast Imaging," *Ultramicroscopy*, **109**, 172–6 (2009).

[20]R. F. Klie, I. Arslan, and N. D. Browning, "Atomic Resolution Electron Energy-Loss Spectroscopy," *J. Electron Spectrosc. Relat. Phenom.*, **143**, 105–15 (2005).

[21]N. D. Browning, M. F. Chisholm, and S. J. Pennycook, "Atomic-Resolution Chemical-Analysis Using a Scanning Transmission Electron Microscope," *Nature*, **366** [6451] 143–6 (1993).

[22]Y. Ito, R. F. Klie, N. D. Browning, and T. J. Mazanec, "Atomic Resolution Analysis of the Defect Chemistry and Microdomain Structure of Brownmillerite-Type Strontium Cobaltite," *J. Am. Ceram. Soc.*, **85** [4] 969–76 (2002).

[23]J. M. Hudspeth, D. J. Goossens, A. J. Studer, R. L. Withers, and L. Noren, "The Crystal and Magnetic Structures of $LaCa_2Fe_3O_8$ and $NdCa_2Fe_3O_8$," *J. Phys.: Condens. Matter*, **21** [12] 124206 (2009).

[24]T. Nakamura, G. Petzow, and L. J. Gauckler, "Stability of the Perovskite Phase $LaBO_3$ (B = V, Cr, Mn, Fe, Co, Ni) in Reducing Atmosphere," *Mater. Res. Bull.*, **14**, 649–59 (1979). □